Low-Cost Albedo Sensing and Thermographic Analysis for Urban Heat Island Monitoring

Jordan P. Sausen[1], Michael D. C. Alves[1], Marcus Polette[1], Mauricio de Campos[1], Gustavo S. Vieira[1], Samuel C. P. T. de Andrade[1]

[1]Escola Politécnica – Universidade do Vale do Itajaí (UNIVALI) – Itajaí, SC - Brazil

{jordan,michaeld,mpolette,mauricio.campos}@univali.br,
{gustavovieira,samuelandrade}@univali.edu.br

Abstract. *Urban heat island effects are strongly influenced by surface radiative properties and urban morphology. This study presents the development and experimental evaluation of a low-cost embedded sensing platform for estimating surface albedo as part of an urban environmental monitoring framework. A field campaign was conducted in Itajaí, Brazil, where infrared thermography was used to characterize thermal contrasts across representative urban locations under sun and shade exposure conditions. In parallel, the proposed sensing platform was used to estimate surface albedo using a low-cost embedded architecture. The results provide an initial characterization of urban termal behavior across representative urban environments. This work represents a preliminary step toward the deployment of IoT-based environmental sensors integrated into a future LoRaWAN infrastructure.*

Keywords: Urban Heat Island; Surface Albedo; Infrared Thermography; IoT Environmental Monitoring.

1. Introduction

The Urban Heat Island (UHI) phenomenon is one of the primary thermal consequences of contemporary urbanization. The replacement of natural surfaces with impermeable, low-albedo materials such as concrete and asphalt, combined with the reduction of vegetation cover, alters the surface radiative balance and intensifies urban heating [Coelho et al. 2024]. Rapid urbanization has significantly altered natural landscapes, modifying the surface energy balance and contributing to the development of the UHI phenomenon, in which urban areas exhibit higher temperatures than surrounding rural regions [Gupta and Kumar, 2025]. The formation of UHI is associated with changes in land use and land cover, reduction of vegetation, and the thermal properties of urban materials [Lefevre et al., 2025]. Urban structures tend to store and re-radiate heat due to their low albedo and high thermal capacity, while anthropogenic heat emissions, urban morphology, and reduced airflow between buildings further intensify surface temperatures.

Despite significant advances in UHI research, important gaps remain in the characterization of urban thermal dynamics at finer spatial scales. Remote sensing and thermographic techniques have been widely applied to investigate spatial thermal variability in urban environments [Chen et al. 2024; Martin et al. 2022], while albedo measurements have demonstrated relevance for evaluating the thermal behavior of urban materials [Li et al. 2013]. However, most studies rely primarily on satellite observations or numerical modeling, with fewer investigations combining low-cost embedded

radiative sensing, thermographic field acquisition, and IoT-oriented environmental monitoring within a unified experimental framework at neighborhood scale.

This study presents the development of a low-cost embedded sensing platform designed to estimate surface albedo through measurements of incident and reflected solar irradiance. Complementary to the radiative measurements, a thermographic campaign was conducted at nine distributed urban locations in Itajaí, Brazil, to identify areas exhibiting stronger surface heating patterns. The proposed framework combines embedded radiative sensing, exploratory field measurements, and thermographic analysis to support the characterization of urban thermal environments. These preliminary observations help identify representative urban surfaces and provide technical insights for the future deployment of distributed environmental sensors within an IoT-based monitoring framework integrated into the IoTec LAB – UNIVALI LoRaWAN network.

2. Methodology

The methodology was structured into three complementary stages: (i) development of an embedded albedo measurement platform for monitoring incident and reflected irradiance; (ii) thermographic field acquisition across representative urban environments; and (iii) computational processing of the resulting dataset using defined thermal contrast metrics. This framework integrates spatial measurements, embedded radiative sensing, and quantitative analysis to support the investigation of UHI dynamics.

2.1 Albedo Measurement Platform

A low-cost embedded platform was developed for continuous monitoring of albedo and adjacent microclimatic variables, as shown in Figure 1. The system was designed under principles of modularity, replicability, and scalability, allowing deployment across different urban surfaces and climatic contexts.

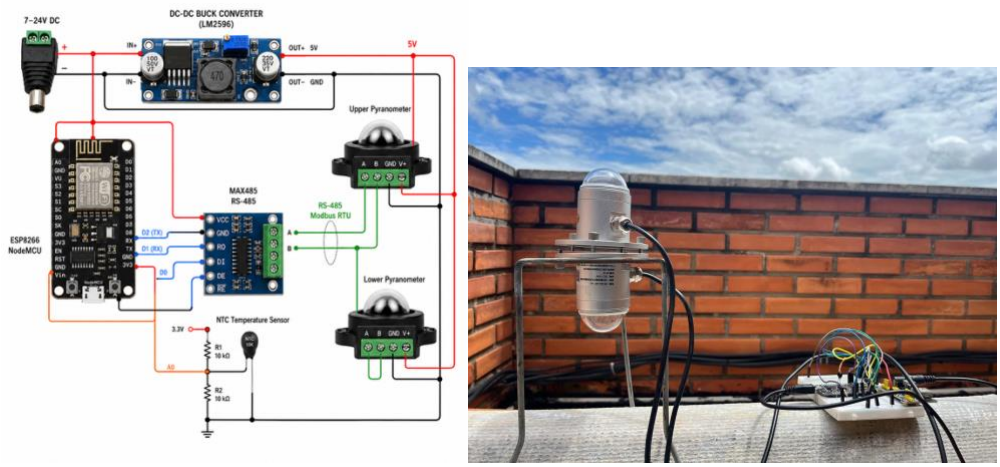

Figure 1. Albedo embedded platform schematic (a) and prototype (b).

The platform consists of two low-cost digital pyranometers communicating via Modbus RTU over an RS-485 bus, enabling simultaneous measurement of incident solar irradiance and irradiance reflected by the monitored surface (Figure 1a). The geometric configuration ensures angular consistency and measurement reproducibility: the upper sensor is horizontally oriented toward the sky to capture global incident irradiance, while the lower sensor is positioned orthogonally to the surface to measure reflected irradiance

(Figure 1b). This arrangement, consistent with validated experimental practices [Li et al. 2013], ensures that the radiative ratio accurately represents the optical behavior of the surface while minimizing angular distortions and local shading effects. An NTC temperature sensor was additionally installed above the monitored surface to record adjacent air temperature continuously. This variable enables assessment of localized atmospheric heating associated with radiative absorption, directly linking incident energy flux to thermal environmental response.

Data acquisition and processing are managed by an ESP8266 (NodeMCU) microcontroller, which handles digital communication with the pyranometers and analog acquisition of the NTC sensor via a 10-bit A/D converter. Communication over RS-485 is implemented using a MAX485 half-duplex transceiver with programmatic control of transmission–reception cycles according to the Modbus RTU protocol, ensuring bus stability and reliable outdoor operation.

Albedo (α) is computed as the ratio between reflected and incident irradiance, as in (1).

$$\alpha = \frac{I_{reflected}}{I_{incident}} \quad (1)$$

A firmware-level plausibility check prevents division when incident irradiance approaches zero, avoiding numerical inconsistencies. Measurements are acquired deterministically at 60-second intervals, providing sufficient temporal resolution to capture radiative and thermal variations throughout the day.

2.2 Field Thermal Acquisition

Strategic data collection points were defined across areas with varying levels of built density, vegetation cover, proximity to water bodies, and predominance of materials such as concrete, asphalt, sand, and vegetation. The selection criteria included urban representativeness, pedestrian circulation intensity, diversity of surface materials, varying solar exposure conditions, and the feasibility of future installation of fixed monitoring sensors for continuous data acquisition. The spatial configuration of sampling points was designed to represent a progressive urban gradient, extending from river-adjacent zones through consolidated central districts toward coastal environments.

Thermal measurements were performed using a portable infrared thermographic camera. At each point, surfaces were classified according to predominant material (concrete, asphalt, vegetation, or sand) and exposure condition (direct solar radiation or shading). For each record, acquisition time, ambient temperature, relative humidity, and maximum, minimum, and central temperatures extracted from the thermographic image were stored. These variables constitute the structured database used for thermal processing and derivation of contrast indicators.

The information extracted from thermal measurements was organized in a structured spreadsheet to enable subsequent computational processing and is made publicly available for future studies [Sausen et al. 2026]. To reduce localized noise and standardize thermal analysis, a mean surface temperature metric estimated from the thermographic extremes was adopted. This approach mitigates localized outliers and facilitates comparability across surfaces and time periods.

Comparing thermal contrasts across heterogeneous urban environments requires normalized indicators capable of reducing the influence of external climatic variability. Two computational indicators were defined using *python*: (i) Thermal Amplitude (ΔT), representing the difference between mean surface temperatures under sun and shade; and (ii) the Thermal Contrast Index (TCI), obtained by normalizing ΔT by ambient temperature at the time of measurement. The TCI enables comparability across heterogeneous environmental conditions and provides an objective metric for urban thermal contrast analysis.

Absolute thermal contrast (ΔT) is defined as in (2), where T_{sol} corresponds to the mean surface temperature under direct solar exposure and T_{sombra} to the mean surface temperature of the same surface under shaded conditions.

$$\Delta T = T_{sol} - T_{sombra} \quad (2)$$

To enable comparability across different environmental conditions, the Thermal Contrast Index (TCI) was defined as in (3), where T_{amb} represents the ambient temperature recorded at the time of measurement, obtained from an automatic weather station (INMET 2026).

$$TCI = \frac{\Delta T}{T_{amb}} \quad (3)$$

The TCI functions as a normalized metric of thermal contrast, reducing the influence of external climatic variability and enabling comparative analysis across distinct sampling points.

3. Case Study

The case study was conducted in the municipality of Itajaí, Santa Catarina, Brazil, with the objective of analyzing urban thermal behavior along a spatial gradient extending from the river margin to the coastal zone. The selection of sampling points sought to represent distinct urban configurations, surface materials, and exposure conditions, enabling the characterization of thermal heterogeneities associated with the urbanization process.

Nine measurement points were defined along an urban–coastal gradient, beginning near the Itajaí-Açu River, crossing consolidated central areas, and extending toward the Praia Brava, a coastal region. This selection sought to represent different land-use patterns, levels of built density, and degrees of surface impermeabilization, as shown in Figure 2.

The spatial configuration of the sampling points reflects distinct urban morphologies:

- Centro (urban core): characterized by high building density and predominance of concrete and asphalt surfaces, with limited vegetation cover, representing the most impermeabilized and consolidated portion of the city.
- Costa (coastal zone): located near the shoreline and influenced by maritime conditions. Despite high solar exposure, this area may experience moderating effects from sea breezes and coastal humidity.

- Rio (river-adjacent region): a socioeconomically vulnerable peripheral area with low arborization and simplified built structures. Its proximity to the river may introduce localized microclimatic moderation.
- Periferia (hillside periphery): also socioeconomically disadvantaged but located near a vegetated hillside, where surrounding vegetation may contribute to localized thermal mitigation.

Figure 2. Case study sampling points.

These contextual differences seek to provide a structural explanation for spatial variations in ΔT, linking thermal contrast to urban morphology, material composition, and environmental context. Thermal measurements were performed using a Hikmicro M30 portable thermographic camera, configured with an emissivity coefficient (ε) set to 0.97, compatible with predominant urban materials such as concrete and asphalt [Wong et al. 2024]. A total of eleven complete sun–shade pairs were obtained and used for the ΔT analysis, which can be found at [Sausen et al. 2026].

The thermal images were processed according to the pipeline described in Section 2, allowing structured extraction of thermal metrics and calculation of the TCI. Complementary to the punctual measurements, an embedded albedo monitoring platform was implemented over a 6 mm thick fibrocement surface representative of the local urban environment, as in Figure 1(b). This material was intentionally selected because fibrocement roofing is widely used in socioeconomically vulnerable residential buildings in Brazil, where low-cost construction materials predominate. Consequently, analyzing its radiative and thermal behavior can provide relevant insights into heat exposure conditions affecting these urban populations, connecting radiative measurements from the embedded platform to the thermographic observations distributed across the municipality.

4. Results

The collected data from the albedo prototype, which can be found in [Alves et al. 2026], enabled both statistical and temporal analysis of solar irradiance under the experimental conditions. A significant reduction in irradiance levels was observed under shading, confirming the direct impact of solar obstruction on the local energy balance. The high temporal resolution of the platform allowed continuous tracking of daily radiative dynamics, demonstrating its suitability for environmental monitoring

applications. Time-series analysis revealed proportional behavior between incident irradiance (upper sensor) and reflected irradiance (lower sensor), as illustrated in Figure 3.

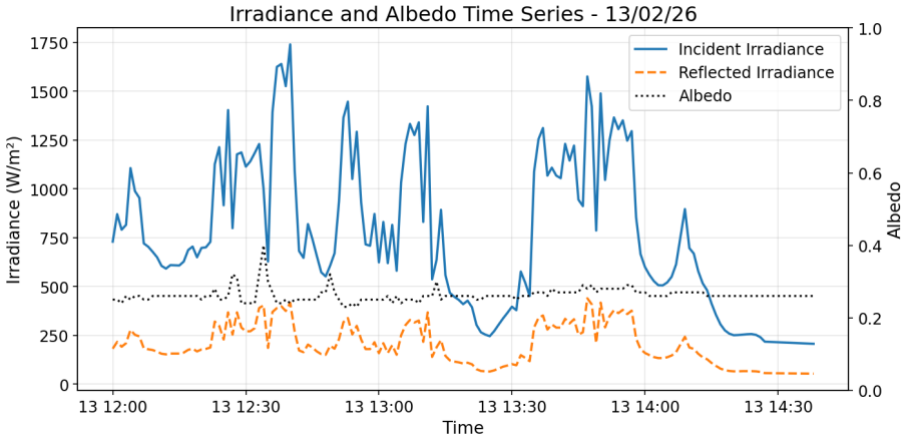

Figure 3. Time series of incident and reflected irradiance.

Pearson's linear correlation yielded a strong positive relationship ($r = 0.796$, $p < 0.001$), confirming that reflected radiation follows incident energy flux. However, the absolute magnitudes differed substantially: peak incident irradiance reached values above 1500 W/m², while reflected values rarely exceeded 400 W/m². This disparity indicates the high absorptivity of the grey fiber-cement surface, which acts as a radiative energy sink, resulting in a median albedo of 0.250.

The temporal behavior shown in Figure 4 confirms the system's sensitivity in capturing daily solar dynamics. The roofing material's low reflectance reinforces the technological relevance of albedo monitoring as a diagnostic tool for urban heat mitigation strategies.

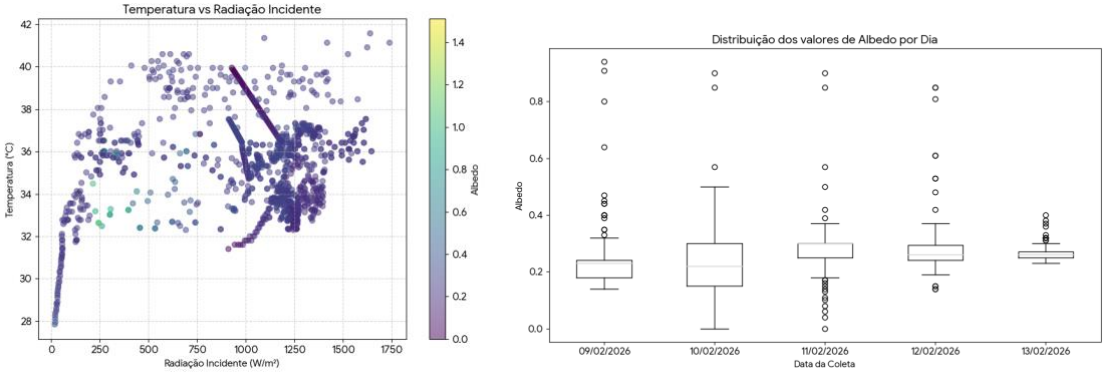

Figure 4. Thermo-radiative behavior analysis. (a) Temporal dispersion between air temperature and incident irradiance. (b) Daily albedo distribution.

Regarding local thermal behavior, the system recorded a mean adjacent air temperature of 35.34°C (±2.26°C). Temporal correlation between air temperature and incident irradiance (Figure 4a) showed weak instantaneous linear association ($r = 0.149$, $p < 0.001$). From a thermodynamic perspective, this result is significant, as it quantitatively evidences material-related thermal latency. Even after solar radiation decreased in the afternoon, local air temperature remained elevated, indicating continued sensible heat release from the surface.

Statistical consolidation of the radiative ratio (Figure 4b) resulted in a median albedo of 0.250 with a stable standard deviation of ±0.088. These values align closely with the reflectance range (0.20–0.35) reported in the literature for naturally weathered cementitious materials, validating the accuracy of the developed instrumentation [Li et al. 2013].

Figure 5 summarizes the thermographic results obtained during the field campaign [Sausen et al. 2026]. Panel (a) presents the distribution of absolute thermal contrast (ΔT) according to surface type, while panel (b) illustrates the spatial variability of ΔT across the investigated urban regions. Figure 5(a) shows that impermeable materials such as asphalt and concrete consistently exhibited elevated thermal contrasts between sun-exposed and shaded conditions.

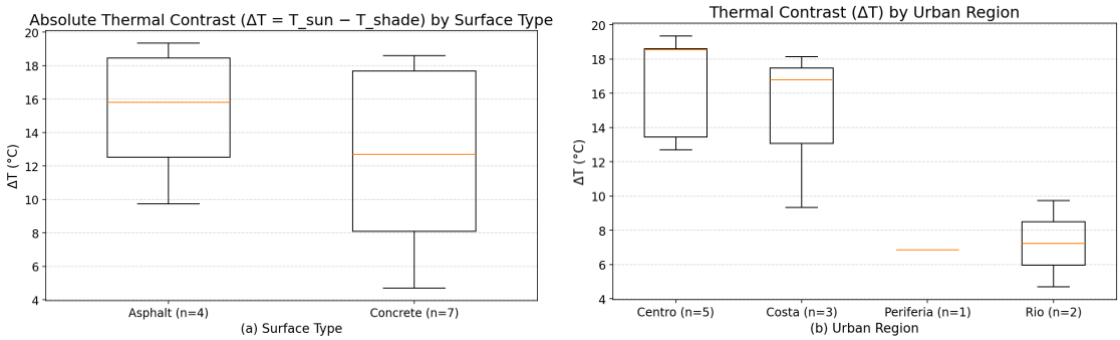

Figure 5. Absolute thermal contrast from field campaign for surface type (a) and urban region (b).

Asphalt surfaces presented the highest median ΔT values, approaching 16 °C, while concrete surfaces displayed slightly lower median values but greater variability across observations. This variability suggests that the thermal response of concrete surfaces is more sensitive to surrounding environmental conditions, including shading patterns, building density, and proximity to vegetation or water bodies. The magnitude of ΔT ranged from moderate contrasts in less dense environments to significantly higher values in heavily impermeabilized zones. This pattern reinforces the role of material properties (particularly absorptivity, heat capacity, and surface reflectance) in governing localized microclimatic behavior.

Figure 5(b) presents the spatial distribution of ΔT across the investigated urban regions. The highest contrasts were observed in the consolidated urban core (Centro), where dense building structures and extensive concrete and asphalt surfaces dominate the landscape. Comparable values were also observed in coastal areas, although with greater dispersion, likely reflecting the moderating influence of maritime airflow and humidity.

In contrast, significantly lower ΔT values were recorded in river-adjacent and peripheral areas. These environments are characterized either by proximity to water bodies or by surrounding vegetation associated with nearby hillsides. Such environmental features appear to reduce surface heating and moderate the thermal contrast between sun-exposed and shaded surfaces.

Table 1 summarizes the TCI statistics by surface type (a) and urban region (b). Asphalt surfaces exhibited higher mean TCI values than concrete, indicating stronger normalized thermal contrasts. Spatially, the highest mean TCI values were observed in the urban core and coastal areas, while river-adjacent and peripheral regions presented

lower contrasts, suggesting a moderating influence of water bodies and surrounding vegetation on local thermal behavior.

Table 1. TCI statistics by surface type (a) and urban region (b).

TCI (a)	Count	Mean	STD	TCI (b)	Count	Mean	STD
Asphalt	6	0,451	0,072	**Centro**	3	0,482	0,061
Concrete	5	0,392	0,089	**Costa**	3	0,438	0,055
				Periferia	2	0,318	0,028
				Rio	3	0,292	0,024

Together, these results indicate that urban thermal contrast is influenced not only by surface material properties but also by broader environmental and morphological conditions. Dense built environments tend to intensify surface heating, whereas proximity to water bodies and surrounding vegetation contributes to moderating local thermal contrasts.

5. Conclusion

This study presented an integrated framework for analyzing urban thermal environments by combining thermographic field measurements with radiative observations obtained from a low-cost embedded albedo sensing platform. The results revealed significant spatial variability in surface heating across the investigated urban regions. Impermeable materials such as asphalt and concrete exhibited the highest absolute thermal contrasts (ΔT), particularly in densely built areas with limited vegetation, while regions near water bodies or vegetated areas showed lower thermal contrasts.

Radiative measurements provided a physical explanation for these patterns. The measured median albedo of approximately 0.25 confirms the low reflectance typical of cementitious materials commonly used in urban environments. Surfaces with low reflectance absorb a larger fraction of incoming solar radiation, which is subsequently released as sensible heat, contributing to the elevated ΔT and Thermal Contrast Index (TCI) values observed in thermographic mappings.

From a technological perspective, the integration of thermographic acquisition with embedded radiative sensing supports the development of scalable urban climate monitoring architectures. The use of LoRaWAN-connected sensing nodes enables continuous acquisition of radiative and microclimatic variables, transforming punctual field measurements into structured time-series datasets. This approach provides a foundation for the future deployment of distributed IoT monitoring systems within the IoTec LAB – UNIVALI LoRaWAN network, supporting long-term analysis of Urban Heat Island dynamics and the development of data-driven mitigation strategies.

6. Use of AI Tools

The authors used generative artificial intelligence tools (ChatGPT, OpenAI) for language editing and text organization. All scientific content, analysis, and conclusions were developed and verified by the authors.

References

Alves, M. D. C., Sausen, J. P., Vieira, G. S., Goedert, A. "Time-Series Dataset of Incident and Reflected Solar Radiation, Ambient Temperature, and Surface Albedo in an Urban Environment", IEEE Dataport, March 19, 2026, https://dx.doi.org/10.21227/q0ap-vr77

Chen, G., Zhou, Y., Voogt, J. A., and Stokes, E. C. (2024) "Remote Sensing of Diverse Urban Environments: From the Single City to Multiple Cities", Remote Sensing of Environment, v. 305, 114108.

Coelho, V. H. R., Patriota, E. G., Bertrand, G. F., Almeida, C. N., Claudino, C. M. A., and Coelho, V. H. R. (2024) "Heat the Road Again! Twenty Years of Surface Urban Heat Island Intensity (SUHII) Evolution and Forcings in 21 Tropical Metropolitan Regions in Brazil from Remote Sensing Analyses", Sustainable Cities and Society, v. 113, 105629.

Gupta, R. and Kumar, A. (2025) "Urban Heat Island Research Using Remote Sensing: A Bibliometric Review with Special Reference to India", Urban Climate, v. 61, 102403.

Instituto Nacional de Metereologia – INMET. Estação de coleta do municipio de Itajaí. Access in Jan/2026. https://tempo.inmet.gov.br/TabelaEstacoes/A868

Lefevre, A., Malet-Damour, B., Boyer, H., and Rivière, G. (2025) "Urban Heat Island in the Tropics: A Review of Advances, Challenges, and Future Directions", City and Environment Interactions, v. 28, 100265.

Li, H., Harvey, J. and Kendall, A. (2013) Field Measurement of Albedo for Different Land Cover Materials and Effects on Thermal Performance. Building and Environment, 59, 536-546. https://doi.org/10.1016/j.buildenv.2012.10.014

Martin, M., Chong, A., Biljecki, F., and Miller, C. (2022) "Infrared Thermography in the Built Environment: A Multi-Scale Review", Renewable and Sustainable Energy Reviews, v. 165, 112540.

Sausen, J. P., Alves, M. D. C., Campos, M., Vieira, G. S., Polette, M. (2026). Field Thermographic Dataset of Urban Surface Temperatures for Urban Heat Island Analysis in Itajaí, Brazil. IEEE Dataport. https://dx.doi.org/10.21227/ma0d-tz96

Wong, T. L. X., Lim, E. L., Hasan, M. R. M., Sougui, O. O., Milad, A., and Qu, X. (2024) "Effectiveness of Heat-Reflective Asphalt Pavements in Mitigating Urban Heat Islands: A Systematic Literature Review", Journal of Road Engineering, v. 4, p. 399–420.

Yang, J., Shi, Q., Menenti, M., Xie, Y., Wu, Z., Xu, Y., and Abbas, S. (2022) "Characterizing the Thermal Effects of Vegetation on Urban Surface Temperature", Urban Climate, v. 44, 101204.